Thin Solid Films 548 (2013) 241–246

Contents lists available at ScienceDirect

Thin Solid Films

journal homepage: www.elsevier.com/locate/tsf

Influence of grain size on the band-gap of annealed SnS thin films

Priyal Jain [a,b], P. Arun [a,*]

[a] Material Science Research Lab, S.G.T.B. Khalsa College, University of Delhi, Delhi, 110 007, India
[b] Department of Electronic Science, University of Delhi, South Campus, Delhi 110021, India

ARTICLE INFO

Article history:
Received 20 March 2013
Received in revised form 23 September 2013
Accepted 26 September 2013
Available online 5 October 2013

Keywords:
Thin films
Chalcogenides
Optical properties

ABSTRACT

Thin films of SnS were fabricated at room temperature on glass substrates by thermal evaporation. X-ray photoelectron spectroscopy confirmed that the films were stoichiometric in nature even after vacuum annealing. X-ray diffraction, Raman analysis and electron microscopy showed that the films were polycrystalline in nature with ortho-rhombic structure and preferred orientation. The only variation due to film thickness and annealing temperature was the grain size. Thus, this provided a chance to investigate the variation in optical properties as a function of the grain size. The energy band-gap and refractive index were estimated using UV-visible absorption spectra. The variation in band-gap with grain size showed blue-shift typical of electron quantum confinement. The effect of crystal ordering on refractive index was also evident by the linear increase of the refractive index with grain size.

1. Introduction

In recent years various reports have appeared discussing the properties of ternary compounds formed from elements belonging to the IV–VI group, such as $Sn_{1-x}Pb_xS$. These reports suggest that ternary materials are the most suited for solar cell applications [1,2]. The properties of these materials strongly depend on their crystal structure which in turn depends on the value of 'x'. In this study, we have studied tin sulphide (SnS) not only since they show similar properties but also because of their low melting point which makes it easy to obtain stoichiometric thin films by thermal evaporation. Tin sulphide (SnS) have shown potential as a holographic or optical data storage medium [3,4]. Also, due to its high absorption coefficient (of the order ~10^4 cm^{-1}) and band-gap ~1.3–1.6 eV [5], SnS films have been used as photo-voltaic devices [6,7]. SnS exists in various crystallized states like orthorhombic [8], tetrahedral (Zinc blende like) [9] or a highly distorted rock–salt (NaCl) structure [10]. However, due to the nature of the tin and sulphur bonding, it forms two-dimensional sheets [11], giving rise to a layered structure with strong intra-planar forces and weak van der Waal forces between the adjacent planes [12,13]. They are hence ideal candidates for obtaining layered films. Films of SnS have been fabricated using various techniques such as thermal evaporation [14], RF sputtering [15], chemical vapour deposition [16], electro-deposition [17], spray pyrolysis [18] and sulphurisation of metallic precursors [19]. It was found that the optical properties of SnS strongly depended on the deposition method used [20–24]. While the maximum band gap (1.78 eV) was reported in films obtained by wet chemical method [8], the lowest band-gap (1.12 eV) was reported for films made by chemical bath deposition [20].

It is known that deposition techniques influences the film's grain size, crystal structure, chemical composition and residual strain which in turn affect the optical properties of the film. In light of the increasing importance of SnS and its potential applications, it becomes important to study the film structure with its band-gap. Thus, in this manuscript we report our studies on vacuum evaporated SnS thin films that were vacuum annealed after fabrication and try to establish a relation between their structural and optical properties.

2. Experimental details

SnS films of varying thicknesses were fabricated by thermally evaporating powdered SnS at vacuum better than ~5.32×10^{-3}Pa in a Hind High Vac (12A4D) thermal evaporation coating unit. The depositions were made on glass microscopy slides maintained at room temperature. SnS powder of 99% purity supplied by Himedia (Mumbai) was used as the starting material. The thickness of the grown films were measured by a Veeco Dektak Surface Profiler (150). The samples were then subjected to post-annealing temperatures under vacuum for 30 min at 373 K and 473 K. The structural, morphological, compositional and optical characterizations were done systematically for both the grown and vacuum annealed films. We report and compare here the structural, morphological, compositional and optical properties of annealed samples of five different thicknesses, 270, 480, 600, 650 and 900 nm. The structural analyses were done using Bruker D8 Diffractometer in the $\theta-2\theta$ mode with Cu target giving X-Ray at 1.5418 Å ($k\alpha_1$ line) operating at 40 kV. In support of the X-Ray Diffraction (XRD) studies, structural analysis was also done with Technai G^2 T30U Twin Transmission Electron Microscope (TEM) at an accelerating voltage of 200 kV. The samples were etched off the glass substrate with the help of a surgical blade and dusted on gold grids. The Raman spectra of the films were

* Corresponding author.
E-mail address: arunp92@physics.du.ac.in (P. Arun).

0040-6090/$ – see front matter © 2013 Elsevier B.V. All rights reserved.
http://dx.doi.org/10.1016/j.tsf.2013.09.089

obtained with Renishaw Invia Raman Microscope using Argon laser beam in the reflection mode. The surface morphology of the samples and their chemical composition was examined with Field Emission Gun-Scanning Electron Microscope (FEG-SEM JSM7600F) operating at 10 kV and its Energy-dispersive X-Ray Spectroscopy (EDX) attachment. Chemical composition of the samples was also examined using Shimadzu's X-Ray Photo-electron Spectroscopy (XPS) (ESCA750 spectroscope) with Al kα X-ray source. The beam energy used for the analysis was 1.49 keV. The binding energy has been referenced with respect to Carbon XPS spectra. Deconvolution of peaks and fitting Gaussian peaks for estimation of area under the graph was done using standard software, Origin 6. The optical properties of the samples were carried out using Systronics UV–VIS Double beam Spectrophotometer (2202).

3. Results and discussion

The Raman spectra were collected from back scattered Ar^{2+} laser. Analysis of all our samples was done maintaining constant beam area, exposure time (30 s) and power (15 mW). All Raman spectra were collected using low power laser since studies on SnS as an optical data storage medium have shown changes induced in it by photo-thermal absorption of light. Fig. (1) shows representative Raman spectra of a 900 nm thick film, before annealing (rt) and after annealing at 373 K and 473 K respectively. All the samples without exception showed two prominent peaks around 170 cm^{-1} and 238 cm^{-1}. The ~170 and 238 cm^{-1} Raman peaks are associated with those of single crystal SnS [8]. Our peak positions are slightly displaced from these positions. These displacements are usually due to the restricted ordering introduced by grain boundaries in polycrystalline samples [25]. The 170 cm^{-1} or the B_{2g} mode's peak corresponds to interaction along the inter-layer 'b' axis, while the 238 cm^{-1} peak is the A_g mode that corresponds to the symmetric Sn – S bonding stretching mode in the a–c plane [26]. It is clear from Fig. (1) that the relative contributions from B_{2g} and A_g do not change on annealing.

Fig. (2) exhibits the X-Ray diffractograms of thin annealed (473 K) SnS films of different thicknesses. Three prominent peaks were seen at $2\theta \sim 31°$, 37° and 43°. The Miller indices of the remaining prominent peaks are also indicated in the figure. These peak positions matched with those reported in ASTM Card No. 83-1758. Two of the peaks, (040) and (131), were also present in the electron diffraction (Selected Area Electron Diffraction, SAED) pattern obtained from TEM. The SnS in our samples thus, exists with orthorhombic unit cell structure [5] with the (040) peak having the maximum intensity. While there are many references in the literature that show (040) peak as the most intense [27,28], others have reported (111) peak to be the most intense [8,29]. This indicates a preferred orientation of the crystallites on the substrate. TEM micrograph of Fig. (3) clearly shows the layered and oriented nature of our SnS films. The planes visible are the (040) planes with inter-planar distances matching the expected 'b/4'. This again underlines how growth technique and conditions influence the character of the SnS films.

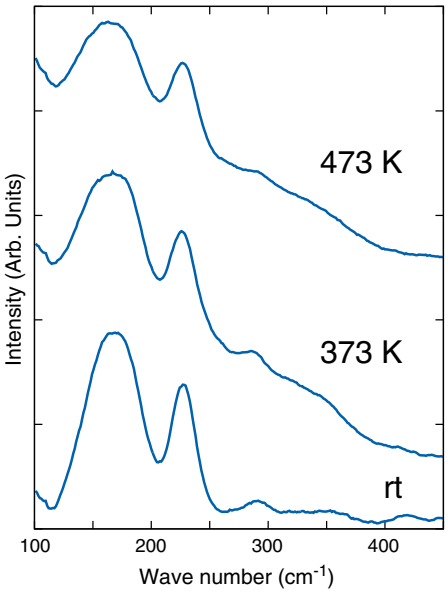

Fig. 1. A representative Raman spectra of a 900 nm thick SnS film before and after annealing at temperatures indicated.

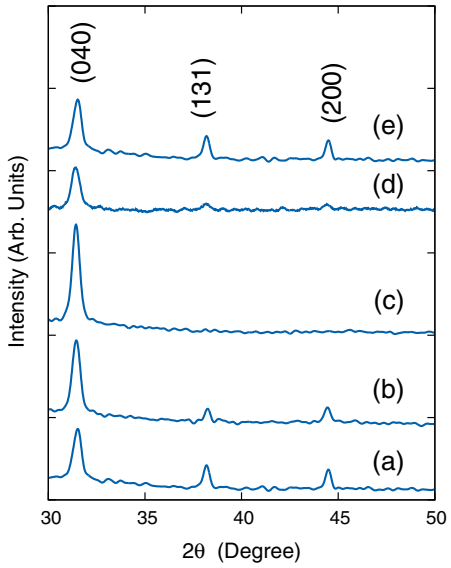

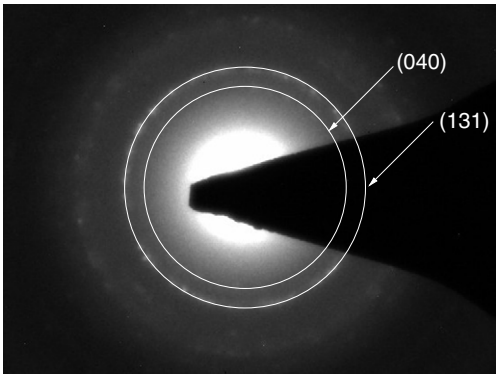

Fig. 2. XRD patterns of SnS films of thicknesses (a) 270, (b) 480, (c) 600, (d) 650 and (e) 900 nm after annealing at 373 K. SAED patterns also showed spots arranged in rings typical of polycrystalline material. The two circles superimposed for easy visualization correspond to the (040) and (131) peaks of XRD.

The lattice parameters 'a', 'b' and 'c' of SnS in single crystal state are given as 4.148, 11.48 and 4.177 Å, respectively. We have evaluated the lattice parameters from the (040), (200) and (131) peak's position using the relation

$$\sin^2\theta_i = Ah_i^2 + Bk_i^2 + Cl_i^2.$$

The lattice parameters of the annealed samples were found to be 4.07 ± 0.002, 11.36 ± 0.01 and 4.45 ± 0.002 Å. The error indicated was calculated from the X-Ray diffractometer's step size used ($2\theta = 0.02°$). They were found to be different from those of SnS in single crystal state. While there is a marginal variation in 'a' and 'b' a significant increase was seen in 'c'. Albanesi et al. [13] have done systematic analysis to understand the effect of changing unit cell size on SnS band-gap. Their study suggested an increase in volume of the unit cell would lead to a lowering in SnS band-gap. We shall return to this when we

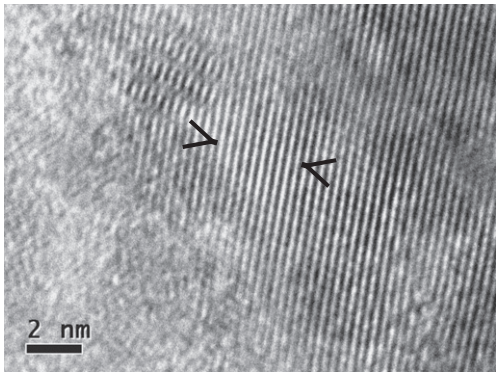

Fig. 3. TEM micrograph shows the layered structure of SnS thin film with parallel planes of (040). Lattice parameter 'b' can also be evaluated from the width of 10 parallel planes enclosed by arrows.

discuss the results of our optical studies. While there is a significant change in the lattice constants (namely 'c') as compared to that of single crystal, we find that they do not change with film thickness or annealing temperature. Fig. (4A) shows all three lattice parameters remaining unaffected with film thickness. Since points coincide, each point in this graph represents samples annealed at 373 K and 473 K. The difference in lattice constant present (c_{obs}) with respect to that given in the ASTM (c_{ASTM}) implies that the grains are in a state of stress with the peaks shifting left compared to those reported in the ASTM, hence we conclude tensile residual stresses are acting within the grains [30]. However, c_{obs} is constant for all the samples hence the same tensile residual stress exists in all the samples. This tensile residual stress thus appears as a background in our study.

While the lattice parameters remain unaltered, the grain size changes with annealing. The grain size reported was calculated using the Full Width at Half Maxima (FWHM) of the diffraction peaks in Scherrer's formula [22,31]. From Fig. (4B), it is clear that there is a persistent increase in grain size with annealing, however this effect is more pronounced in thinner films. The grain size increases from 12 nm to 25 nm in the 270 nm films while this increase in grain size with annealing temperature is impeded for thicker films (Fig. 4B).

SnS are layered compounds with zig-zagged molecules of SnS forming layers. These layers stack one on top of the other along the 'b' axis [32] with weak van der Waal 'inter-planar' forces acting between the layers. The layers themselves because of the zig-zagging have finite thickness and along the 'b' axis have strong 'intra-planar' forces acting within it. Ehm et al. [33] have shown that application of pressure decreases inter-planar distances along 'b' axis without disturbing intra-planar spacing. As stated above, the Raman B_{2g} peak represents vibrations along the 'b' axis. Fig. (5) shows the variation in Raman peak position of annealed samples. While the A_g peak remains fixed at 226.5 cm^{-1}, the B_{2g} peak shows a systematic shift to a higher wavenumber with increasing film thickness. It would appear that thinner films with larger grain size have vibrations taking place at lower wave-number than thicker films with smaller grains. The Raman peak's position and its FWHM is a rich source of information. While it does give information on the structure, the corroborative XRD study showing no variation in lattice parameters implies variation in Raman spectra is indicative of something else. Literature on Raman Analysis has shown variation of FWHM to be a measure of phonon confinement [34,35] with shift in peak position related to grain size [25,36-39] and nature of defect on the grain boundaries [34]. A shift to higher wavenumber is indicative of smaller grain size. Hence, the results of XRD and Raman analysis put together suggest that annealed SnS thin films have large grains with grain size decreasing as the annealed film thickness increases. This is best understood from Fig. (6).

The results shown in Fig. (4B) are also reflected in the Scanning Electron Microscope's micrographs (Fig. 7). The film of 480 nm thickness showed significant increase in grain size and grain density when

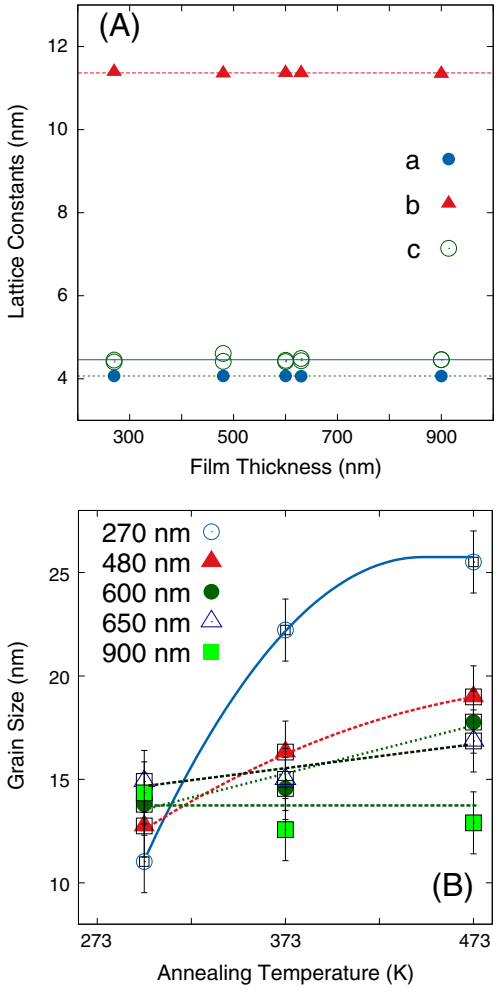

Fig. 4. Graphs show the variation in (A) lattice constants with film thickness (annealed) films. Diameter of representing points is of the order of error in the determination of lattice parameters. (B) Grain size with annealing temperature. Bars indicate the ±1.5 nm error in determination of grain size. These results were obtained from the X-ray diffraction patterns.

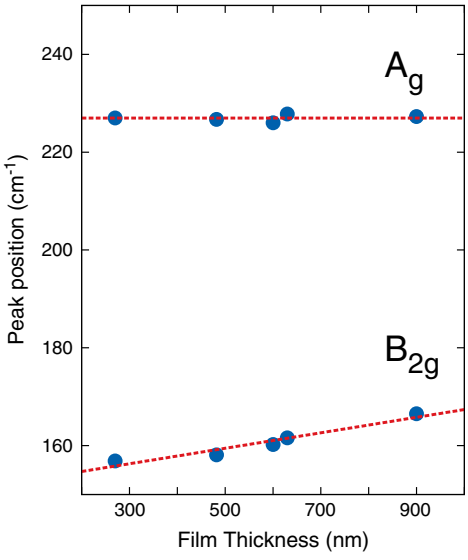

Fig. 5. The variation in Raman A_g and B_{2g} peak positions of annealed (373 K and 473 K) SnS films with film thickness.

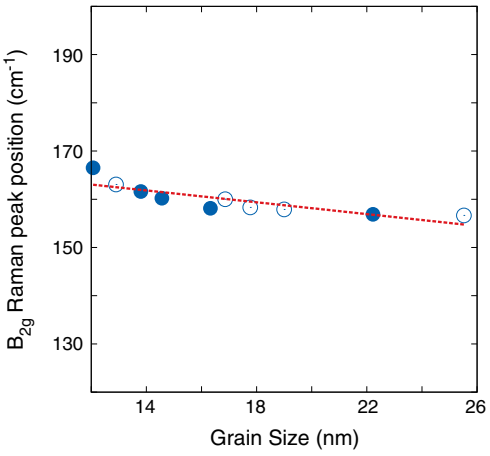

Fig. 6. The B_{2g} peak position of Raman spectra varies with grain size. The graph shows shift of Raman peak to lower energy level with increasing grain size. The filled circles represent data of samples annealed at 373 K while the unfilled circles represent those that were annealed at 473 K.

annealed at higher temperature as compared to the 900 nm thick film. Comparing the 900 nm thick films annealed at 373 K and 473 K respectively, we do not find such improvement in grain size or density as was inferred from the XRD analysis. Also, the elongated flake like grains lying parallel to the substrate corroborates the preferred (040) orientation observed in TEM and XRD.

Fig. (8) shows EDX of 900 nm thick film annealed at 473 K. Even after annealing at 473 K no oxidation is evident (Si and O is from glass substrate). This is evidently due to the fact that annealing was done in vacuum (6.65 Pa). Besides showing the lack of oxidation, we also investigated the chemical composition of our samples using XPS. XPS analysis becomes important because sulphur with tin can exist either as SnS or SnS_2. Fig. (9) shows the Sn ($3d_{5/2}$) and S (2p) XPS peaks of a 480 nm thick annealed sample. These are representative of all our annealed samples. While a single Gaussian peak fits to the sulphur peak, the shoulder in the Sn peak suggests a second state of Sn. The small Gaussian peak at this shoulder indicates a free tin while the dominant second Gaussian peak is of tin in bonding with sulphur. The amount of sulphur in bonding with tin can be evaluated with the knowledge of area under the curves/peaks (Δ) using [40]

$$\frac{n_S}{n_{Sn}} = \left(\frac{\Delta_S}{\sigma_S}\right)\left(\frac{\sigma_{Sn}}{\Delta_{Sn}}\right) \quad (1)$$

where n_S and n_{Sn} are the number of sulphur and tin atoms in bonding per cm^3 area. The ease with which the elements release electrons is given by photoelectric cross-section factor, σ. σ_S and σ_{Sn} are the sensitivities or cross-sectional factors of sulphur and tin respectively. We have used the cross-section values of sulphur's $2p_{1/2}$ and tin's $3d_{3/2}$ peaks as given by Band et al. [41]. We obtain $n_S/n_{Sn} \approx 1.1$ from the area under the peaks of sulphur and tin (in bonding) Fig. 9. Within experimental error we may conclude our samples are of SnS. At this point, it should be understood that the XPS scans were obtained for the surface from where sulphur might have escaped giving some free Sn. Hence, within the surface, we may safely conclude that our studied annealed samples are compositionally stoichiometric SnS.

Based on the above results, it would be interesting to study the optical properties of these samples. Since the lattice parameters and residual tensile stress on the grain's bulk remain the same with only grain size and to an extent grain density varying in the samples, the study should reveal the contribution grain size has on the properties like band gap, E_g.

The optical absorption and transmittance spectra of all the samples were obtained in between wavelength range 300–900 nm. The absorption spectra were typical with absorption increasing near band-edge. The band-gap can be evaluated using the absorption coefficient (α)

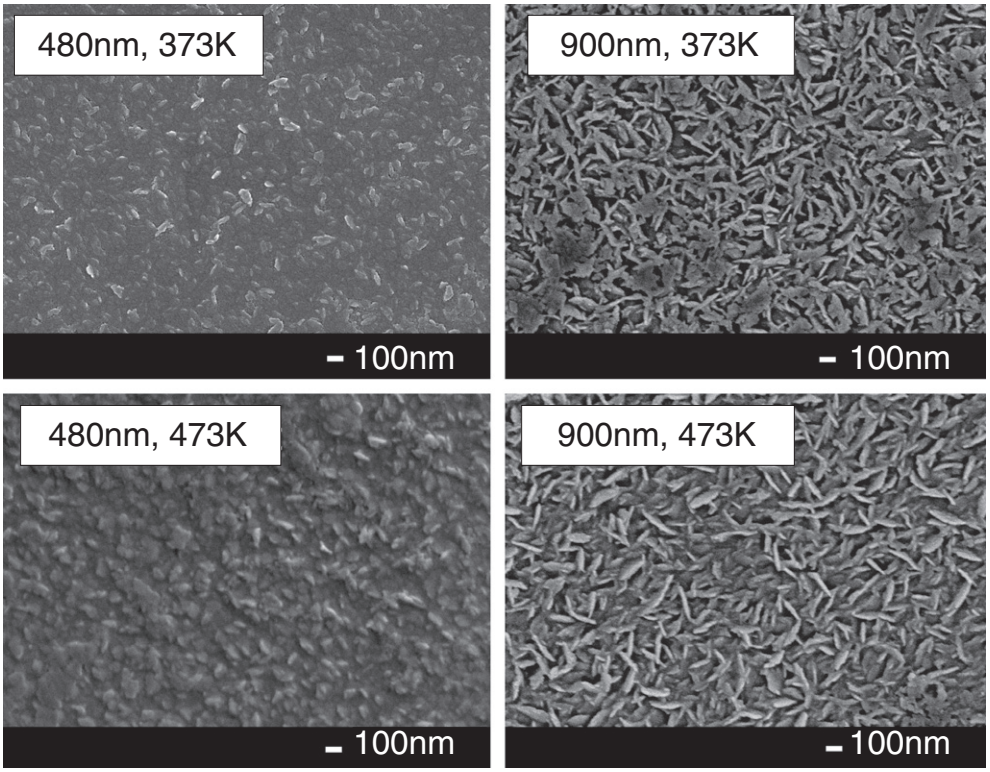

Fig. 7. SEM micrographs show grain size improvement in thinner film (480 nm) when annealed at higher temperature. However, the 900 nm films show no variation in grain size on annealing.

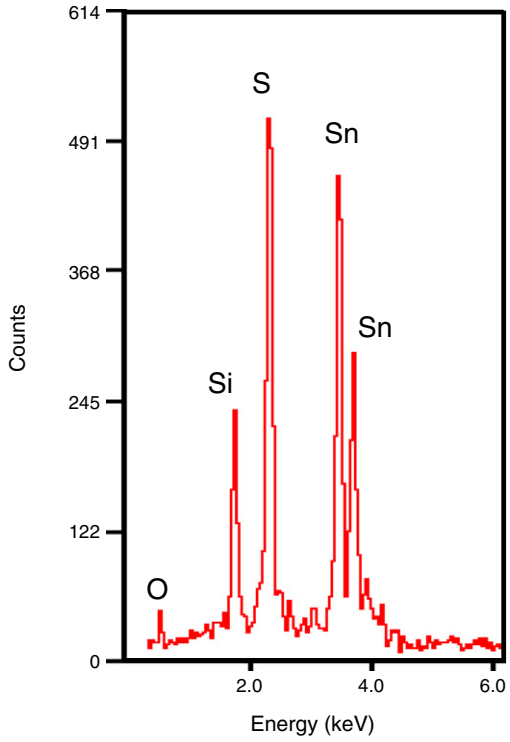

Fig. 8. EDX spectroscopy of a larger area of 900 nm thick film, vacuum annealed at 473 K, show no oxidation of the sample. The minimal silicon and oxygen present are from the substrate.

obtained from the UV-visible spectra. The band-gap is obtained using the relation [42]

$$\alpha h\nu = \left(h\nu - E_g\right)^n$$

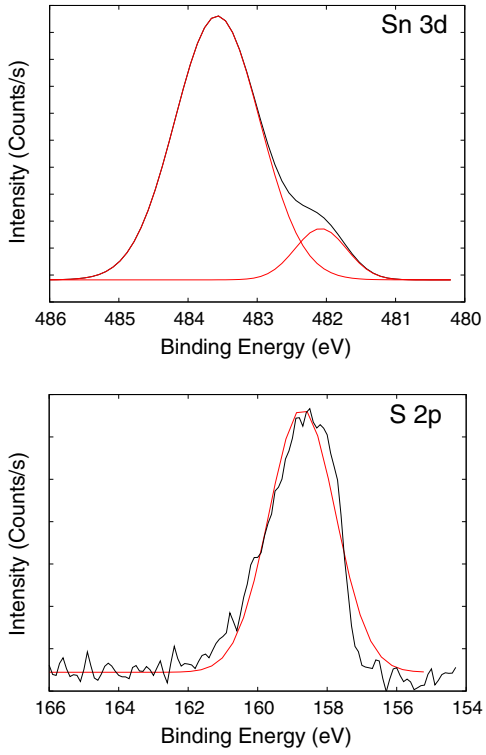

Fig. 9. XPS spectra of tin and sulphur of a 480 nm thin film annealed at 373 K.

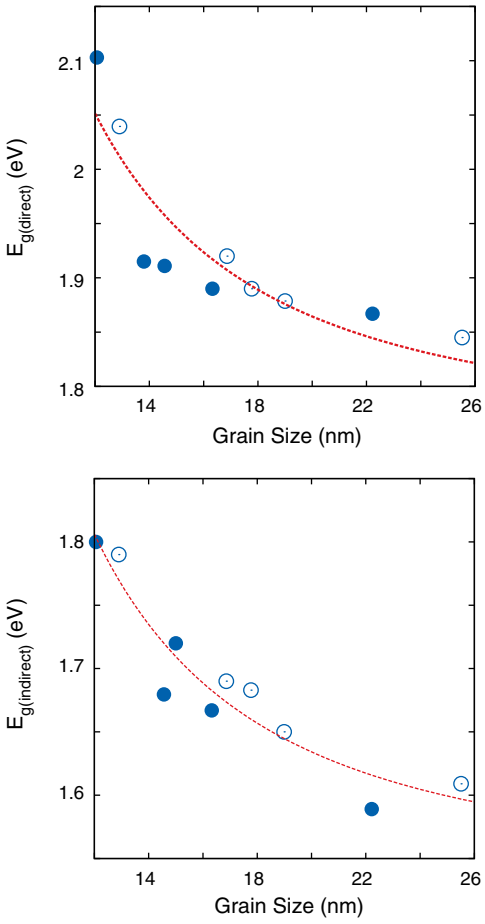

Fig. 10. The band-gap (direct and indirect) of annealed SnS films was found to be a function of grain size. The filled circles represent data of samples annealed at 373 K while the unfilled circles represent those that were annealed at 473 K. The calculations based on Eq. (2) are represented by the continuous line.

where 'n = 1/2' and 'n = 2' are for direct and indirect allowed transitions respectively. On extending the best fit line on the linear part of the curve between $(\alpha h\nu)^{1/n}$ and $h\nu$, the point where the line cuts the 'X-axis' gives the energy band-gap of the sample. Using this method, we have evaluated both direct and indirect band-gaps for all the samples. Both theoretical [13,43] and experimental [7,8,23,28,44,45] works are divided on the nature of band-gap in SnS. Xing et al [45] hence have concluded that it has both direct and indirect band-gaps. It is for this reason, we have evaluated both direct and indirect band-gaps for all our samples.

As discussed earlier, the lattice parameters remained unchanged for annealed films, hence it can be conclusively said that the band-gap variation here is not caused by the lattice defects. The band-gap of SnS films strongly depends on the deposition process and the film parameters like the film thickness. SnS amorphous film of thickness 1000 nm grown on a glass substrate by spray pyrolysis has a band-gap of 1 eV [18]. While film grown by vacuum evaporation was found to be nano-crystalline with band-gap varying between 1.15 and 1.3 eV. The variation in band-gap was found to be related to the distance between the source and the substrate [29]. Films grown on ITO substrates by pulsed electro-deposition were polycrystalline in nature with band-gap being 1.34 eV [27]. Polycrystalline films grown by chemical bath deposition on glass substrates of 290 nm thickness also possess low band-gap (1.15 eV) [20]. While the films grown with RF sputtering technique are also nano-crystalline, they have very high band-gaps varying from 1.3 to 1.7 eV [15]. A recent study [46] on SnS polycrystalline thin films grown by thermal evaporation reports SnS band-gap between 2.15 and 2.28 eV. Clearly, polycrystalline SnS films have higher band-gaps

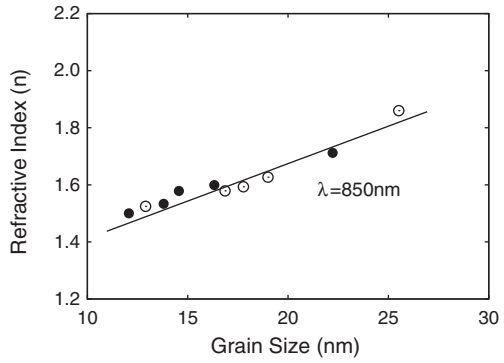

Fig. 11. The variation of SnS film's refractive index at λ = 850 nm with grain size. The filled circles represent data of samples annealed at 373 K while the unfilled circles represent those that were annealed at 473 K.

compared to their amorphous counterparts. There are comments in literature that higher contents of sulphur (SnS_2) would lead to higher band-gaps. However, XPS results show that our samples were stoichiometric SnS.

Fig. (10) shows the grain size dependence of the band-gap. Both the band-gaps decrease with the increasing grain size. This study shows that on annealing, thinner films have larger grains. The large grain size gives the annealed samples a lower band-gap. Thicker films however, have smaller grains and an enhanced band-gap. The band-gap of a sample is broadly affected by its chemical composition, crystal structure, grain size and defects. Of all these contributing parameters, except for grain size, all other parameters remain constant. While the larger volume of the unit cell leads to a background low E_g (~1.8 eV) as explained by Albanesi [13], decreasing grain size contributes to an increase in E_g of the vacuum annealed SnS samples. The band-gap's variation with grain size due to quantum confinement has the quantitative form [47]

$$E_g^{nano} = E_g^{bulk} + \frac{\hbar^2\pi^2}{2Mr^2} \quad (2)$$

where 'r' is the radius of the nano-particle and 'M' is the effective mass of the system. The solid line of Fig. (10) shows a good fit of Eq. (2) to our experimental data points. The result again reiterates influence of both the lattice parameters (via E_g^{bulk}) and grain size on the band-gap of SnS.

The variation in grain size also affects the film's refractive index. We have calculated the refractive index of our films using Swanpoel's method [48]. Fig. (11) shows the variation in the film's refractive index for λ = 850 nm with grain size. The refractive index increases with increasing grain size, showing some dependency on range of crystal ordering. These results show that the optical properties of SnS such as band-gap and refractive index are strongly dependent on the grain size. The grain size is controllable by film thickness and annealing temperature giving us control to tailor the properties of SnS films as per our requirement.

4. Conclusion

Thin films of SnS were fabricated by thermal evaporation on microscopy glass slides at room temperature. These films when annealed in vacuum at 373 K and 473 K developed a tensile strain along the lattice 'ac' plane. The magnitude of this tensile strain was independent of the film thickness and annealing temperature. Thus, the contribution of this tensile strain remained as a constant background throughout this study. The film thickness and annealing temperature, however, play an important influencing role on the sample's grain size. We conclude from our results that the band-gap, E_g (direct and indirect), of nanocrystalline SnS films invariably depends on the grain size due to quantum confinement. Also, the refractive index of the films decreases with decreasing grain size.

Acknowledgement

Authors are thankful to the Department of Science and Technology for funding this work under research project SR/NM/NS-28/2010. We are also grateful to Dr. Chhaya Ravi Kant, Department of Applied Sciences, IGIT (GGS-IP University, Delhi) for extending necessary assistance. Thanks are also due to Dr Rajdeep Singh Rawat and Mr Usman Ilyas, Nanyang University, Singapore for XPS measurements.

References

[1] G. Wagner, R. Kaden, V. Lazenka, K. Bende, Phys. Status Solidi A 9 (2011) 2150.
[2] K. Bente, V.V. Lazenka, D.M. Unuchak, G. Wagner, V.F. Gremenok, Cryst. Res. Technol. 45 (2010) 643.
[3] M. Radot, Rev. Phys. Appl. 18 (1977) 345.
[4] S.G. Patil, R.H. Tredgold, J. Pure Appl. Phys. 4 (1971) 718.
[5] K.T.R. Reddy, N.K. Reddy, R.W. Miles, Sol. Energy Mater. Sol. Cells 90 (2006) 3041.
[6] Z. Wang, S. Qu, X. Zeng, J. Liu, C. Zhang, F. Tan, L. Jin, Z. Wang, J. Alloys Compd. 482 (2009) 203.
[7] H. Noguchi, A. Setiyadi, H. Tanamora, T. Nagatomo, O. Omato, Sol. Energy Mater. Sol. Cells 35 (1994) 325.
[8] S. Sohila, M. Rajalakshmi, C. Ghosh, A.K. Arora, C. Muthamizhchelvan, J. Alloys Compd. 509 (2011) 5843.
[9] C. Gao, H. Shen, T. Wu, L. Zhang, F. Jiang, Mater. Lett. 64 (2010) 2177.
[10] A.N. Mariano, K.L. Chopra, Appl. Phys. Lett. 10 (1967) 282.
[11] T. Jiang, G.A. Ozin, J. Mater. Chem. 8 (1998) 1099.
[12] P.M. Nikolic, P.L. Miljkovic, B. Mihajlovic, B. Lavrencic, J. Phys. C: Solid Status Phys. 10 (1977) L289.
[13] L. Makinistian, E.A. Albanesi, Comput. Mater. Sci. 50 (2011) 2872.
[14] M.M.E.I. Nahass, N.M. Zeyada, M.S. Aziz, N.A.E.I. Ghamaz, Opt. Mater. 20 (2002) 159.
[15] K. Hartman, J.L. Johnson, M.I. Bertoni, D. Recht, M.J. Aziz, M.A. Scarpulla, T. Buonassis, Thin Solid Films 519 (2011) 7421.
[16] M.T.S. Nair, P.K. Nair, Semicond. Sci. Technol. 6 (1991) 132.
[17] A. Ghazali, Z. Zainal, M.Z. Hussein, A. Kassim, Sol. Energy Mater. Sol. Cells 55 (1998) 237.
[18] B. Thangaraju, P. Kaliannan, J. Phys. D. Appl. Phys. 33 (2000) 1054.
[19] K.T.R. Reddy, P.P. Reddy, Mater. Lett. 56 (2002) 108.
[20] C. Gao, H. Shen, L. Sun, Appl. Surf. Sci. 257 (2011) 6750.
[21] K.T.R. Reddy, P.P. Reddy, P.K. Datta, R.W. Miles, Opt. Mater. 17 (2001) 295.
[22] G.H. Yue, D.L. Peng, P.X. Yan, L.S. Wang, W. Wang, X.H. Luo, J. Alloys Compd. 468 (2009) 254.
[23] M. Devika, N.K. Reddy, K. Ramesh, K.R. Gunasekhar, E.S.R. Gopal, K.T.R. Reddy, Semicond. Sci. Technol. 21 (2006) 1125.
[24] A. Ortiz, J.C. Alonso, M. Garcia, J. Toriz, Semicond. Sci. Technol. 11 (1996) 243.
[25] K.A. Alim, V.A. Fonoberrov, A.A. Baladdin, Appl. Phys. Lett. 86 (2005) 053103.
[26] H.R. Chandrasekhar, R.G. Humphreys, U. Zwick, M. Cardona, Phys. Rev. B 15 (1977) 2177.
[27] G.H. Yue, W. Wang, L.S. Wang, J. Alloys Compd. 474 (2009) 445.
[28] F. Jiang, H. Shen, C. Gao, B. Liu, L. Lin, Z. Shen, Appl. Surf. Sci. 257 (2011) 4901.
[29] M. Devika, N.K. Reddy, D.S. Reddy, S.V. Reddy, K. Ramesh, E.S.R. Gopal, K.R. Gunasekhar, V. Ganesan, Y.B. Hahn, J. Phys. Condens. Matter 19 (2007) 1.
[30] A.L. Patterson, Phys. Rev. 56 (1956) 978.
[31] T.H. Sajeesh, A.R. Warrier, C.S. Kartha, K.P. Vijayakumar, Thin Solid Films 518 (2010) 4370.
[32] S. Schlecht, L. Kienle, Inorg. Chem. 40 (2001) 5719.
[33] L. Ehm, K. Knorr, P. Dera, A. Krimmel, P. Bouvier, M. Mezouar, J. Phys. Condens. Matter 16 (2004) 3545.
[34] K. Kitahara, T. Ishii, J. Suzuki, T. Bessyo, N. Watanabe, INT J. Spectrosc. 2011 (2011) 1.
[35] H.C. Choi, Y.M. Jung, S.B. Kim, J. Vib. Spectrosc. 37 (2005) 33.
[36] J.S. Zhu, X.M. Lu, W. Jiang, W. Tian, M. Zhu, M.S. Zhang, X.B. Chen, X. Liu, Y.N. Wang, J. Appl. Phys. 81 (1997) 1392.
[37] M. Rajalakshmi, A.K. Arora, B.S. Bendre, S. Mahamuni, J. Appl. Phys. 87 (2000) 2445.
[38] C.L. Yang, J.N. Wang, W.K. Ge, L. Guo, S.H. Yang, D.Z. Shen, J. Appl. Phys. 90 (2001) 4489.
[39] L. Guo, S. Yang, C. Yang, P. Yu, J. Wang, W. Ge, G.K.L. Wong, Appl. Phys. Lett. 76 (2000) 2901.
[40] D. Briggs, Handbook of X-ray and Ultra-violet Photon-electron Spectroscopy, PerkinElmer Corporation, Phys. Electronics Division, 1978.
[41] L.M. Band, Y.I. Kharitonov, M.B. Trzhaskovskaya, At. Data Nucl. Data Tables 23 (1979) 443.
[42] K. Kamano, R. Nakata, M. Sumita, J. Phys. D. Appl. Phys. 22 (1989) 136.
[43] G.A. Tritsaris, B.D. Malone, E. Kaxiras, J. Appl. Phys. 113 (2013) 233507.
[44] M. Calixtro-Rodriguez, H. Martinez, A. Sanchez-Juarez, J. Campos-Alvarez, A. Tiburcio-Silver, M.E. Calixto, Thin Solid Films 517 (2009) 2497.
[45] X. Gou, J. Chen, P. Shen, Mater. Chem. Phys. 93 (2005) 557.
[46] S. Cheng, G. Conibeer, Thin Solid Films 520 (2011) 837.
[47] L.E. Brus, J. Chem. Phys. 80 (1984) 4403.
[48] R. Swanepoel, J. Phys. E 16 (1983) 1214.